 https://doi.org/10.3311/PPci.28772


**Periodica Polytechnica Civil Engineering**, 68(4), pp. 1350–1366, 2024

# Meso-scale Study of Bond Behavior between Ribbed Steel Rebar and Fiber-reinforced Cementitious Composite Considering Rebar Rib Geometry

Reza Akbarifar[1], Alireza Mortezaei[1*], Ali Babaei[1]

[1] Civil Engineering Department, Semnan Branch, Islamic Azad University, 35131-19111 Semnan, Iran
[*] Corresponding author, e-mail: a.mortezaei@semnaniau.ac.ir

Received: 13 January 2024, Accepted: 29 June 2024, Published online: 16 July 2024

**Abstract**

This study aims to develop a meso-scale finite element approach to investigate the pull-out behavior of ribbed steel rebar and fiber-reinforced cement composites. We considered separately the three phases of steel fibers, cement composite matrix, and rebar within the meso-scale finite element model. A random distribution of fibers was generated in the matrix based on the geometric characteristics of the fibers and their volume fraction. By employing the interfacial transition zone (ITZ) model, the interaction between rebar and fibers with cement composite was simulated. Experimental pull-out tests were conducted to determine the parameters of the model. A meso-scale finite element model was validated and the effect of rebar diameter and fiber volume fraction on the bond behavior of rebar with fiber-reinforced cement composites was examined. In accordance with the experimental results, the bond-slip curve obtained with the meso-scale finite element model can be divided into five areas: non-slip, slight slip, splitting, decreasing, and residual. Additionally, it can be observed that fiber-free cement composites fail by splitting, whereas specimens containing fibers fail by sliding. This numerical model is therefore able to predict and estimate the influence of a variety of parameters on the pull-out response between fiber-reinforced cement composite and ribbed bar and failure mechanisms without the need for expensive and time-consuming testing.

**Keywords**

fiber-reinforced cement composite, ribbed rebar, pull-out test, meso-scale finite element model

## 1 Introduction

Cement-based composites with their unique properties, including low manufacturing cost, availability of production resources in nature, adaptability to several environments and climatic conditions, and relatively low weight, have made this material of great importance in the construction industry [1–3]. One of the most important advances in cement-based composite technology is the development of using different types of fibers [4–6]. The new generation of this material is called fiber-reinforced cement composite (FRCC), with mechanical properties greatly enhanced compared to normal concretes [7]. In the meantime, the bond between FRCC and rebar shows a significant role in the behavior of structural members when exposed to static and dynamic loads [8]. Thus, due to the lack of information regarding the bond behavior of rebar in contact with FRCC, it seems crucial to investigate this matter.

Utilizing fibers in FRCC raises ductility, impact strength, flexural strength, tensile strength, and strength against dynamic loads and rupture [9–11]. Besides, using different types of fibers decreases the probability of premature rupture of concrete, prevents crack propagation, and develops the softening zone in the concrete matrix [12, 13]. Garcia-Taengua et al. [14] studied the effects of concrete compressive strength, concrete cover, rebar diameter, slenderness, fiber content, and length of the steel fibers on the pull-out load of rebar. Pi et al. [15] experimentally investigated the influence of brass coating and nano-$SiO_2$ on the bond strength between fibers and FRCC. The effect of fibers on reinforcing the cement composite was experimentally investigated by Lin and Ostertag [16] studied the interaction between steel rebar and FRCC. In their study, hybrid fibers consisted of steel fibers and PVA with

**Cite this article as:** Akbarifar, R., Mortezaei, A., Babaei, A. "Meso-scale Study of Bond Behavior between Ribbed Steel Rebar and Fiber-reinforced Cementitious Composite Considering Rebar Rib Geometry", Periodica Polytechnica Civil Engineering, 68(4), pp. 1350–1366, 2024. https://doi.org/10.3311/PPci.28772

different lengths and diameters. Their investigation showed that depending on the amount of fiber, several types of failure, including sliding failure and crack growth, occur in the specimens. Zhou and Qiao [17] studied the bond performance of epoxy-coated rebar and FRCC and provided an analytical model to calculate the bond-displacement curves. They extracted the bond-displacement curves for different specimens and investigated the influence of various parameters on the pull-out load utilizing the pull-out test [18]. Wang et al. [19] experimentally investigated the pull-out performance of polymer rebar from basalt fiber-reinforced cement composite. Their study results reveal that rebar diameter insignificantly affects the bond strength and average slip relative to fiber content.

Even though empirical research can be employed to determine the properties of fiber-reinforced composites, particularly cement composites, the process requires the use of complex experimental procedures and costly equipment. As a result, computational modeling techniques can be quite effective in determining the mechanical properties of composites [20–22]. In the study of concrete's mechanical behavior, it is not realistic to assume the homogeneity of the material. As a concrete specimen under loading conditions cracks, it transitions from a continuous state to a discrete state. Therefore, it is no longer possible to apply classical finite element methods in such circumstances [23–25]. The modeling of concrete can generally be classified into three distinct scales, namely macro-scale, meso-scale, and micro-scale. Concrete is traditionally treated in classical finite element models as a homogeneous material at the macro-scale. At the meso-scale, concrete consists of coarse aggregate, mortar matrix, and an interfacial transition zone (ITZ) [26]. It is possible to accurately predict the development of damage within a multi-phase material by using an explicit meso-scale model that allows for a direct description of the material heterogeneity [27–30]. A laboratory study was conducted by Komasi et al. [31] to determine the optimal mixing scheme for pervious concrete with an additive of microsilica fume. Khani et al. [32] examined the elastic properties of composites reinforced with helical carbon fiber deploying the finite element method. Esmaeili and Andalibia [33] developed a three-dimensional meso-scale finite element model to analyze the mechanical performance of fiber-reinforced polymer composites. They applied the three-dimensional nonlinear finite element method to conduct the simulations and simulated the interaction between fibers and matrix with the assistance of the cohesive zone model (CZM). Their study reveals that the bond between fibers and concrete matrix depends on several factors such as the direction of fibers, length of fibers, their geometric shape, and strength of the matrix. Ayatollah et al. [34] proposed meso-scale modeling to obtain nonlinear properties of polymer nanocomposites under tensile, flexural, and torsional loads. In their model, the interface phase is continuously modeled, and different Young's modulus is taken into consideration. The results of their study illustrate that the mechanical properties of the interface between fibers and matrix, affect the stiffness of nanocomposite. Nonetheless, the aspect ratio of fibers significantly affects Young's modulus. Yao et al. [35] experimentally and numerically examined bond strength between Silane-coated steel fibers and cement mortar. They used a three-line bond-slip model to simulate the cohesive behavior and proved that this model is relatively accurate. Alizadeh et al. [36] investigated the influence of graphite particles on the mechanical performance under tensile loading using the multi-scale numerical method. In one of the most recent studies in this field, Esmaeili et al. [30] examined the pull-out behavior between fibers and polymer composite considering the various geometric shapes of fiber ends, utilizing the meso-scale finite element method. Their study proposed a new algorithm for the random distribution of particles within the matrix, and by considering the interaction between fibers and matrix, they extracted the results using ABAQUS commercial code. Furthermore, in some studies, the ITZ model in the form of the finite element method has been utilized to model the fiber-matrix interface zone and investigate the origin and growth of separation in this zone. Bouhala et al. [37] have determined the failure parameters of composites utilizing an inverse method based on the ITZ model and the finite element technique. In this technique, the thickness of interfacial elements is assumed to be zero, and by defining failure properties, the separation behavior of fibers and matrix can be simulated. Considering the accuracy of this method, the interface between fibers and matrix will be simulated with the ITZ model in the present study.

This study addresses a significant gap in the existing literature concerning the mechanical simulation of pull-out behavior between rebar and Fiber-Reinforced Cementitious Composite (FRCC). While previous research in this area has been limited, our study aims to investigate the key factors influencing the bond strength between FRCC and ribbed steel rebar by simulating pull-out behavior. What sets our work apart is the utilization

of a meso-scale model, a novel approach that allows for a detailed examination of the bond properties between ribbed rebar and FRCC. For the first time, we have developed a finite element simulation method using the ABAQUS commercial code, which considers the influence of rebar rib geometry and the random distribution of fibers within the cement matrix. By incorporating the interfacial transition zone (ITZ) model and calibrating its parameters based on experimental pull-out tests, we have achieved a more accurate representation of the interaction between microfibers/rebar and concrete. Our study further explores the impact of various parameters, such as fiber volume fraction and rebar diameter, on the bond properties of rebar and FRCC through systematic simulations. Finally, through rigorous validation against experimental data, we have demonstrated the reliability and effectiveness of our proposed meso-scale model, highlighting its potential for advancing understanding in this field.

## 2 Experimental tests

### 2.1 Mixing process and materials

This section illuminates the process of building the FRCC and also the characteristics of the materials used. The cement-based composite mixing scheme developed in the study by Chao et al. [38] has been utilized to examine the pull-out behavior of the rebar. Cement composite consists of Portland cement type III, type F fly ash, silica fume, steel fibers, and water. Silica fume has an average particle size of 0.45 μm, density of 2650 kg·m$^{-3}$, and $SiO_2$ content of 98.9%. Also, the ratio of cement to superplasticizer is 0.24. To make fiber-reinforced cement composite, dry materials, including fly ash, cement, and silica fume are mixed at 80 rpm for 4 minutes. The superplasticizer was dissolved in water, then added to the mixture, and mixed at 150 rpm for 10 minutes. Finally, the steel fibers were added and mixed at 120 rpm for 5 minutes. The compressive strength of fiber-free cement composite was acquired on cubic specimens with dimensions of 150 × 150 × 150 mm equal to 72 MPa. The split tensile test is an indirect way of evaluating the tensile test of concrete. The ASTM C496/C496M-17 [39] split cylinder testing procedure is the standard test to determine the tensile strength of concrete. Steel fibers have a diameter of 0.5 mm, and a length of 14 mm, which is shown in Fig. 1.

**Fig. 1** Straight steel micro-fibers

The investigations in this study were conducted for the S340 reinforcement steel grade by the ISIRI 3132 standard [40], which is the most common rebar grade in the Iranian market. Ribbed rebars with a diameter of 12 mm and yield strength of 448 MPa are used. The fibers have a tensile strength of 2420 MPa and yield stress of 430 MPa. Elastic modulus and Poisson's ratio of the fibers are 208 GPa and 0.28, respectively. The rebars were utilized for pull-out tests according to ASTM A615/A615M-24 standard [41]. In this research, the stress-strain curve of the rebar is extracted utilizing a steel rebar tensile strength experimental testing according to ASTM E8/E8M-24 standard [42], which is illustrated in Fig. 2 (a). A load-controlled direct tension test was performed on steel rod specimens with a length of 50 cm and a test zone of 30 cm. Testing is performed on a universal testing machine (Fig. 2 (b)) using a constant load rate of 0.3 MPa/s until the samples failure completely (Fig. 2 (c)).

### 2.2 Rebar pull-out test

This study carried out a central pull-out test to obtain the interphase strength properties between the rebar and the FRCC matrix. The pull-out test involves pulling out the rebar from the concrete. The pull-out load on one side and the displacement on the other end of the rebar are measured. The present study manufactured pull-out specimens according to RILEM-CEB RC6 [43]. Bond-part steel rebar with a bond-breaker is located in the middle of the concrete specimen. A PVC tube is employed around the steel rebar to remove the issue of the confining pressure provided by the frictional restriction at the reaction plate. This type of test is performed to evaluate direct bond strength and does not represent the stress conditions of a reinforcing. Based on Fig. 3, the bond length is $l_e = 5d$, the dimensions of the concrete specimen are 150 mm × 150 mm, the length $l_e$ + 35 mm is selected, and the length of the PVC pipe is 35 mm. Two pull-out test samples were made. In the first sample, concrete without fibers was used and its results were used to determine the interface constants of rebar and concrete. The second sample is made of fiber-reinforced concrete, the results of which are used to verify the proposed meso-scale finite element model.

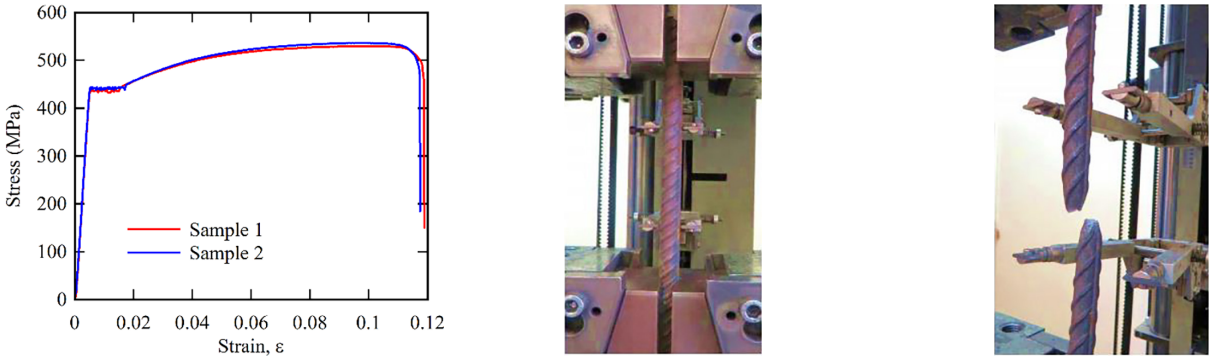


(a) (b) (c)

**Fig. 2** (a) Rebar stress-strain curve, (b) test setup for uniaxial tensile testing of steel rebar, and (c) fracture modes of steel rebar after tensile test


(a) (b) (c)

**Fig. 3** (a) Dimensions for the pull-out specimen (unit: mm), (b) pull-out sample without fiber, and (c) pull-out sample with fiber

Based on Fig. 4, a tensile testing mechanism with load capability of 80 kN and displacement rate of 0.15 mm/min has been utilized to conduct fiber and rebar pull-out tests. To record displacement, the LVDT displacement sensor is used, which is placed on the upper surface of the concrete specimen according to Fig. 4 (a), and measures the comparative displacement between the steel frame and the concrete specimen. The difference between the two comparative displacements indicates the slip between the rebar and the concrete. Finally, the load-slip curve for the FRCC specimens with 0 and 1% volume fraction of fibers is obtained by performing experimental tests. To evaluate the pull-out behavior of the straight steel fibers in cement mortar, a full dog-bone-shaped specimen was fabricated and tested. Its geometry is shown in Fig. 4 (b); it had a cross-sectional area of 20 × 20 mm$^2$ and a length of 75 mm.

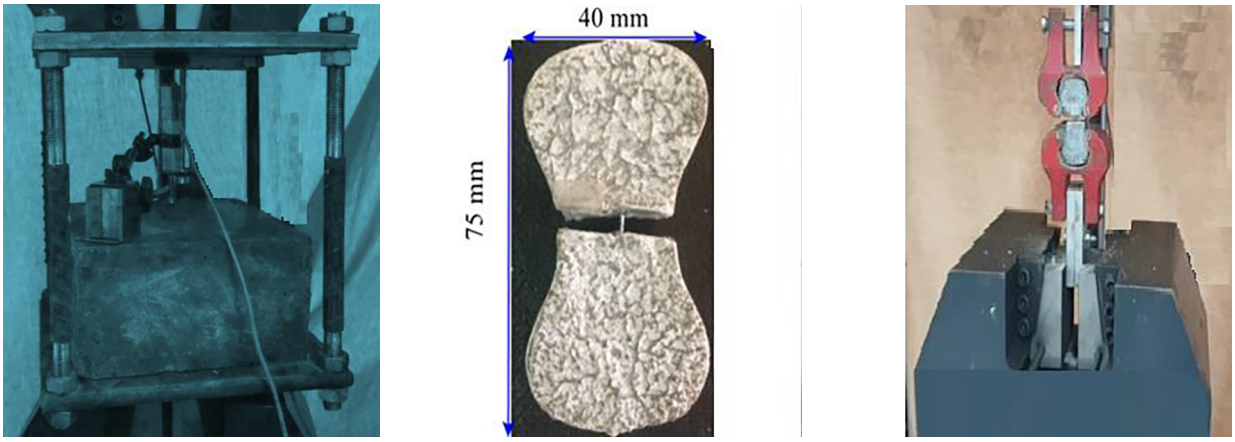


(a) (b) (c)

**Fig. 4** (a) Rebar pull-out test setup, (b) Fiber pull-out setup and sample

## 3 Meso-scale finite element model

In our study, we proposed a novel approach for simulating the pull-out behavior between ribbed rebar and FRCC using finite element analysis. While our method builds upon existing formulations within the framework of finite element modeling, it introduces novel aspects in terms of parameterization, boundary conditions, and analysis techniques tailored specifically to the study of bond properties between these materials. We employed the ABAQUS commercial code to implement these finite element simulations, aiming to accurately capture the intricate interactions at the interface between ribbed rebar and FRCC. This approach allowed us to investigate the bond properties comprehensively and analyze the influence of various factors such as rebar rib geometry and fiber distribution on the pull-out behavior. We acknowledge that further details regarding the specific aspects of our proposed finite element method could enhance clarity and understanding, and we will ensure to provide a more explicit description in the revised manuscript.

The primary aim of this work is to improve a finite element method to analyze the pull-out behavior between rebar and FRCC. In meso-scale finite element modeling, FRCC is made up of three parts: steel microfiber, cement matrix, and the ITZ between them. With the established meso-scale numerical model of FRCC, the three-dimensional meso-scale finite element approach is established in four main phases. First, the cylindrical shaped fibers are generated. Second, the space enclosed by fibers is meshed by cubic elements and the mortar is formed by meshing among these phases and the boundaries of the domain. Third, the ITZ is created by embedding the zero-thickness elements into the mesh structure at the interface of steel rebar and fibers with mortar. In addition, the boundary conditions for the simulation as well as the properties of the materials and applied loads are defined.

Unlike most of the numerical studies in which the rebar is simulated as a flat bar, in this work, the geometry of the treads is also considered in the finite element simulation. Fig. 5 shows the geometric dimensions of the pull-out sample and rebar along with the cross-section of its treads. In the numerical simulation, the geometric and mechanical characteristics of rebar and concrete have been obtained by conducting experimental tests. In the following, the details of the numerical simulation are presented.

### 3.1 Random generation of fibers

In the proposed meso-scale finite element modeling, steel fibers are simulated as cylinders of a certain diameter and length. Furthermore, the cement composite matrix is considered a rectangular cube with homogeneous and isotropic materials with mechanical properties determined by

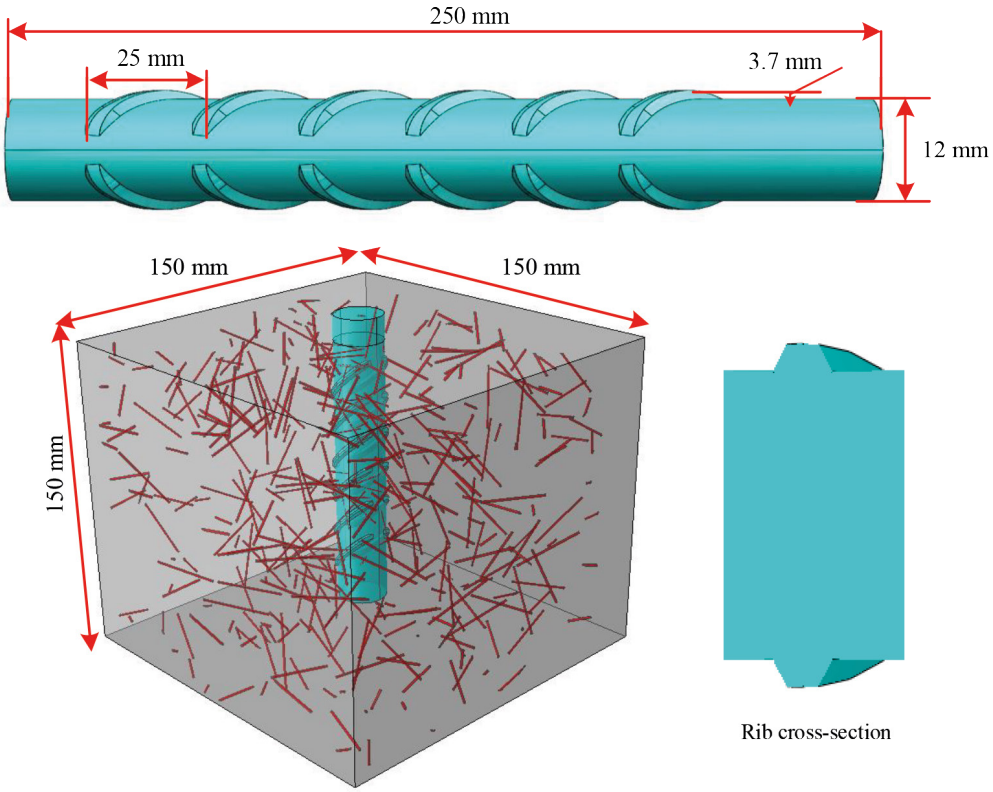


**Fig. 5** Dimensions of the pull-out sample and ribbed rebar

performing experimental tests on the specimens. To form the geometric model of the fiber composite, the fibers are generated by random distribution in the model, and then the volume of the fibers is removed from the cement matrix.

In the present study, to create a three-dimensional geometric model of fiber distribution within the cement matrix, a code was written in MATLAB, as well as the ABAQUS commercial code. The fibers are generated in cylindrical shape inside the matrix in the three-dimensional model according to their geometric shape. In this kind of simulation, the force applied to the fibers is transferred to the matrix. Based on this, the mechanical behavior of the FRCC can be examined. Fig. 6 displays the geometric models of the random distribution of the fibers generated utilizing the mentioned algorithm for 1% and 2% volume fraction of the fibers, respectively. As can be observed, the three-dimensional geometry permits the fibers to be in different orientations, lengths, and positions. This also shows the position of the fibers on the XY plane. It is observed that the fibers are randomly placed in the cement matrix, and therefore, produce a realistic distribution of fibers in the matrix.

### 3.2 Definition of the ITZ model

Concrete is conventionally perceived as a three-phase composite comprising coarse aggregates, mortar, and the ITZ between them. When conducting finite element modeling on a meso-scale, it becomes imperative to employ appropriate meshes that effectively discretize the three constituents of concrete. Given its status as the weakest component, the ITZ assumes a pivotal role in concrete behavior. However, meshing the ITZ presents a formidable challenge owing to its significantly reduced thickness. Employing solid elements to represent the ITZ at such minute scales would result in prohibitively dense finite element meshes. As an alternative strategy, this study opts to model the ITZ using zero-thickness interface elements.

The cohesive zone model theory was used to characterize the damage behavior on the meso-scale structure of FRCC [44]. In this numerical simulation, the damage process of the interfacial transitional zone was described by the linear-exponential traction separation law. The schematic diagram of the FE model with cohesive elements is shown in Fig. 7. Based on its exponential model, the

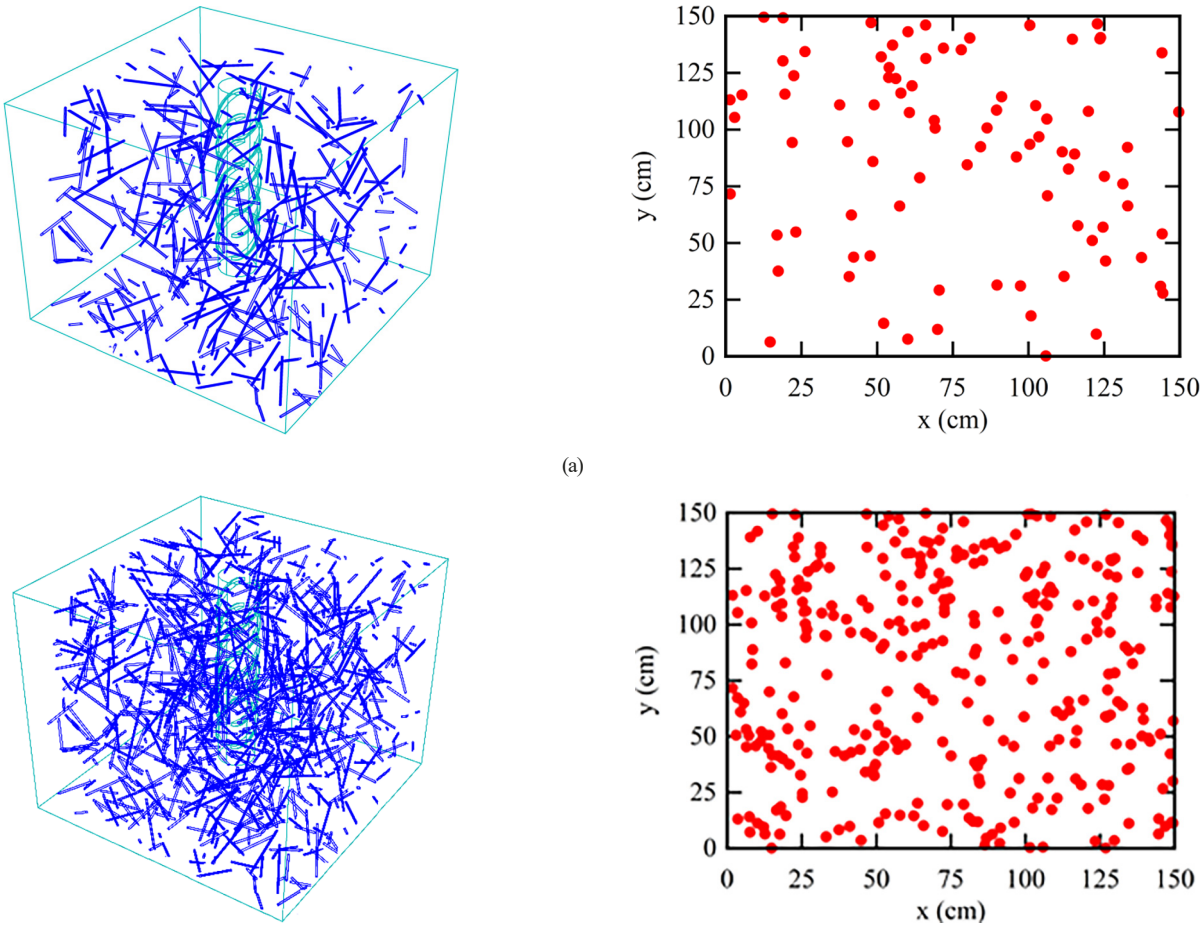


**Fig. 6** Geometry of the microfibers with random distribution with (a) volume fraction of 1% and (b) volume fraction of 2%

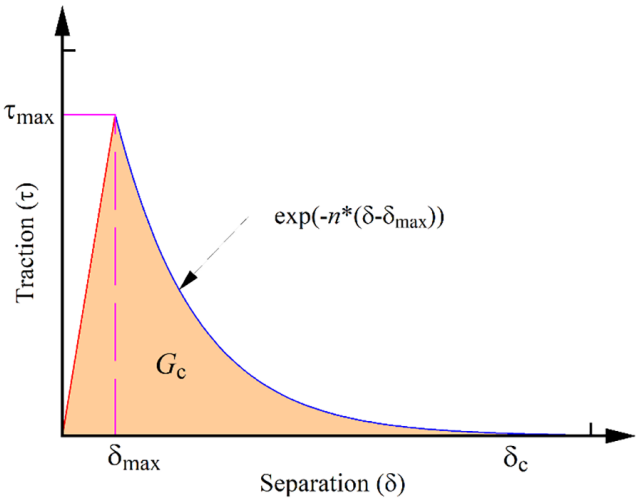


**Fig. 7** Linear-exponential traction separation law of the ITZ model

separation law simulates the mechanical behavior of the contact surface. As illustrated in Fig. 7, the contact surface behavior is supposed to be linear in the absence of any failure. This linear behavior vanishes with the onset of failure. This model assumes that all the mechanisms of macrostructure and failure process can be considered in three ways. These ways involve bond strength ($\tau_{max}$), critical separation distance $\delta_{max}$, the parameter $n$ indicating the exponential softening in the failure zone. In addition, $G_c$, is interfacial failure energy.

In the present case, the loading on the fibers is in the combined mode. Therefore, both tangential and normal contact stress components contribute to failure energy. The form of failure energy is expressed as:

$$\left(\frac{G_n}{G_{cn}}\right)^2+\left(\frac{G_t}{G_{ct}}\right)^2=1 \tag{1}$$

where $G_{cn}$ and $G_{ct}$ are the critical normal and tangential cohesive fracture energies; $G_n$ and $G_t$ are the normal and tangential failure energies, respectively, and are equal to the area under the load-displacement curve, determined by the following relations:

$$G_n=\int_0^{\delta_c}\tau_n(\delta)\,\mathrm{d}\delta \tag{2}$$

$$G_t=\int_0^{\delta_c}\tau_t(\delta)\,\mathrm{d}\delta\,. \tag{3}$$

After calibrating the numerical model with the results of the experimental tests and determining the ITZ parameters between the fibers and the cement composite, the finite element model of the pull-out behavior is examined.

### 3.3 Simulation of rebar pull-out from FRCC

The test of rebar pull-out from FRCC is simulated in 3D with the utilization of ABAQUS commercial code. In this research, for the first time, ribbed rebar is simulated. Fig. 8 shows the finite element model with the boundary conditions and loading. Based on the empirical test, the upper surface of the concrete specimens is completely bound. The displacement up to a maximum of 20 mm is applied to the upper surface of the rebar. Since the areas around the rebar are more sensitive, finer meshing has been used in these areas. In the finite element models, modified 10-node three-dimensional tetrahedral elements (C3D10M) are utilized for meshing, and a nonlinear dynamic method is used to analyze the problem. The proper dimensions of the elements are determined after checking the grid independence. The results were obtained for elements

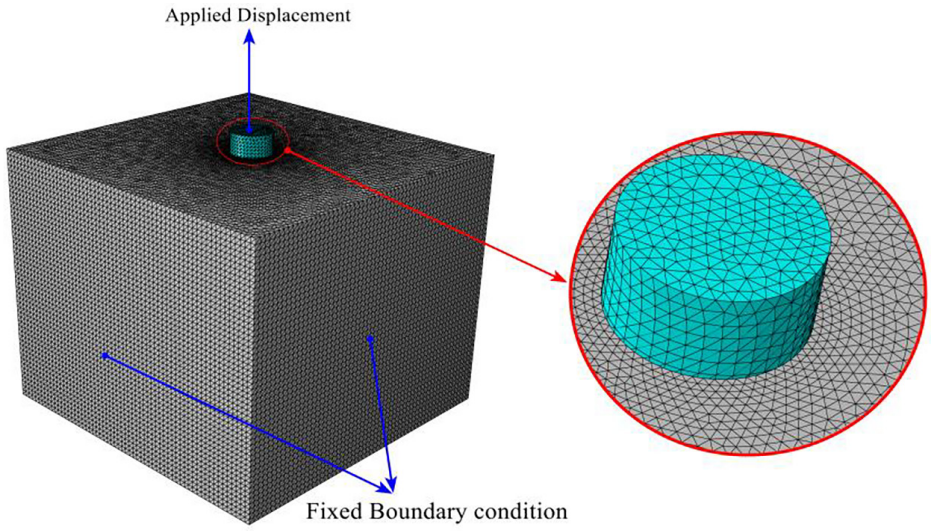


**Fig. 8** Meso-scale finite element model of pull-out test with boundary conditions and loading

with dimensions of 0.1 mm for rebar, 1.2 mm for cement matrix, and 0.01 mm for steel fibers. Additionally, to consider more realistic assumptions in three-dimensional models, the cohesive element was taken into account to define the chemical adhesion between the rebar and the FRCC. To validate the numerical models, the initial results of the finite element were compared with the experimental results of the fiber-free cement composite, and then the finite element models were calibrated.

### 3.4 Material properties

Steel fibers and rebar are modeled using a perfect elastic-plastic material model. Since rebar in concrete has a relatively high mechanical strength and the load level is relatively low, it is reasonable to assume that it behaves like an elastic plastic material that is damage-free, whereas mortar, fibers, and ITZ are considered the weaker constituents. For the mortar-solid elements, the damage variables are defined according to the concrete damage plasticity (CDP) model. For the zero-thickness ITZ elements, the damage variables are defined according to the traction-separation relationship. The parameters required for the CDP model in ABAQUS are the dilation angle, eccentricity, the ratio of biaxial to the uniaxial compressive yield stresses ($f_{b0}/f_{c0}$), and the viscosity parameter. Using the trial and error method and calibrating numerical results with experimental results, these values have been determined for cement mortar. A stress-strain curve for cement mortar has also been determined using experimental tensile and compressive tests. Table 1 shows these results, and these values are entered directly into the software. The mechanical properties of the rebar are also input based on the stress-strain curve shown in Fig. 2 (a). Furthermore, the mechanical characteristics of steel fibers are determined by the catalog of the manufacturer. There is a detailed description of all this information in Tables 1 and 2.

In this context, distinct interfacial properties are attributed to the interactions between rebar and mortar, as well as between fiber and mortar. A more exhaustive investigation, extending beyond the confines of the current study, should aim to encompass analyses such as the examination of single fiber pull-out behavior, considering all the variables that impact the interaction between fiber and matrix. The principles governing the constitutive responses of Concrete Damage Plasticity (CDP) and cohesive elements have been extensively documented in the ABAQUS user manual and reiterated in various scholarly works [45]. Thus, the key model configurations are merely pointed out in this section. Regarding input parameters, the mechanical properties of concrete from the compressive strength test of mortar, rebar from the tensile test, and fibers using the manufacturer's catalog have been used. Also, the characteristics of the fiber-mortar interface were obtained from the single fiber pull-out test and the rebar-mortar interface characteristics were obtained from the rebar pull-out test of concrete without fibers. All material input parameters used for rebar, fiber, cement mortar (CDP), and ITZ (cohesive element model) are given in Tables 1–3.

**Table 1** Material specification of the components for finite element analysis input

| Cement mortar (CDP model) | | | | | | | |
|---|---|---|---|---|---|---|---|
| $\rho$ (kg/m$^3$) | $E$ (GPa) | $\upsilon$ | Dilation angle | Eccentricity | $f_{b0}/f_{c0}$ | $f_{co}$ (MPa) | Viscosity |
| 1820 | 21.3 | 0.2 | 35° | 0.1 | 1.16 | 45 | 0.0005 |
| Steel rebar | | | | Steel fiber | | | |
| $\rho$ (kg/m$^3$) | $E$ (GPa) | $\upsilon$ | $\sigma_y$ (MPa) | $\rho$ (kg/m$^3$) | $E$ (GPa) | $\upsilon$ | $\sigma_y$ (MPa) |
| 7850 | 205 | 0.28 | 448 | 7850 | 208 | 0.28 | 430 |

Note: $\rho$, $v$, $E$, and $\sigma_y$ are density, Poisson's ratio, Young modulus and yield stress, respectively.

**Table 2** Concrete compression and tension behavior based on experimental results

| Concrete compression hardening | | Concrete tension stiffening | |
|---|---|---|---|
| Strain | Stress (MPa) | Strain | Stress (MPa) |
| 0 | 16.50 | 0 | 0.00 |
| 0.001 | 71.63 | 0.000148 | 4.67 |
| 0.002 | 33.48 | 0.000392 | 3.17 |
| 0.003 | 18.55 | 0.000635 | 2.61 |
| 0.004 | 8.35 | 0.000879 | 2.29 |
| 0.005 | 3.37 | 0.001122 | 2.08 |
| 0.006 | 1.40 | 0.001366 | 1.92 |

**Table 3** The ITZ model parameters to define the interaction among steel microfibers, ribbed rebar and FRCC

| | $\tau_{max}$ | $\delta_{max}$ | $G_{cn}$ | $G_{ct}$ | $n$ |
|---|---|---|---|---|---|
| Steel fiber | 5.47 MPa | $3.08 \times 10^{-3}$ mm | 0.025 MPa·mm | 0.41 MPa·mm | 0.32 |
| Steel rebar | 130 MPa | $1.64 \times 10^{-3}$ mm | 1.14 MPa·mm | 1.85 MPa·mm | 1.23 |

## 4 Results and discussion

To investigate the dependency between mesh size and element type, a mesh sensitivity study was conducted on the pull-out test. To verify the accuracy of the finite element models, different models consisting of elements of sizes 0.01–2 mm were used. The results of this study indicate that refinement of the mesh results in changes in the pull-out response, as shown in Fig. 9. When finer meshes are used, displacement increases as expected, but when finer meshes are used, results do not differ significantly. The mesh size and accuracy of the model are sufficient, which indicates that the mesh size is appropriate. In this paper, all other comparisons are made concerning fine mesh to ensure the accuracy of the numerical study.

Using the single fiber and rebar pull-out experimental tests, the ITZ model parameters are determined. Then, the effect of different parameters on the pull-out behavior and bond strength of the ribbed rebar with the FRCC is investigated. The interaction between the fibers and the cement matrix was carried out by employing contact constraints and defining the ITZ elements. The ITZ model parameters were determined so that the load-displacement curve acquired from the finite element model closely matches the experimental results of the pull-out test of the steel rebar (with a 12 mm diameter). After calibrating the results, the ITZ model parameters are obtained according to Table 3.

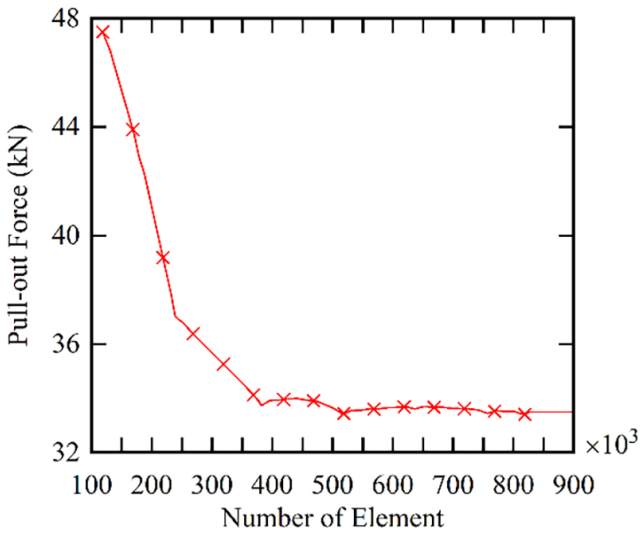


**Fig. 9** Influence of mesh size on the pull-out force in FRCC with 1% of steel fiber

Given the Table 1, the load-slip curve of the final numerical model and the experimental test results of specimens with 0 and 1% volume fraction of the fibers are presented in Fig. 10 (a). There can be observed a favorable overlap both in curve shape and the maximum pull-out load between the experiments and the numerical model. There is less than 2% error in the maximum pull-out load results between the finite element model and the experimental test. Furthermore, the finite element model can be utilized for studying the impact of various parameters on the pull-out behavior between the rebar and the FRCC. Fig. 10 (b) shows the comparison between the pull-out load-displacement curve obtained from numerical simulation and the results of the steel fiber pull-out test. When the bond strength $\tau$ of the cohesive element is taken as 130 MPa and the fracture energy $G_c$ is taken as 1.85 MPa·mm, the peak pull-out load obtained by the simulation is 9.42 N, the displacement corresponding to the peak pull-out load is 0.87 mm, and the experiment results are 9.83 N and 0.91 mm, with errors of 4% and 4.3%, respectively. Therefore, this paper presents numerical simulation results that are in good agreement with experimental results.

The load-slip curves in Fig. 10 show that for the same characteristics of the rebar, the application of the fibers substantially enhances bond load and bond strength between the rebar and the cement composite. For instance, for rebar with a diameter of 12 mm, the maximum bond load in the presence of 0 and 1% volume fraction of the steel fibers is 25.6 kN and 32.9 kN, respectively, indicating that the utilization of 1% fibers increases the bond strength by about 28%. The primary reason for this can be attributed to the increase in mechanical loads as a result of adding fibers to FRCC. According to the stress distribution, two modes of failure are predictable. If the shear stress in the cement matrix switches between the rebar ribs exceeds the shear strength of the cement matrix, the rebar will move outwards, and the failure will be pull-out of the rebar from the cement matrix. In case the tensile stresses surpass the tensile strength of the concrete, radial cracks will form in the cement matrix around the rebar, causing the cement matrix coating around the rebar to shatter and the cement matrix to rupture. At this stage of the bond behavior, the impact of friction on the capacity of the ultimate bond load

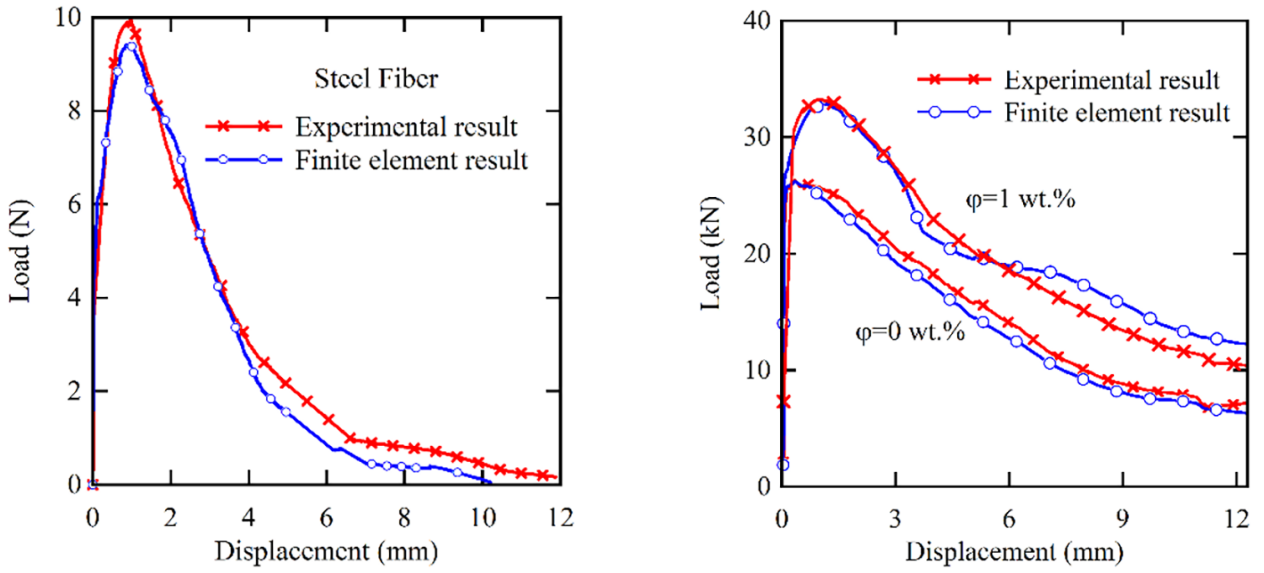


(a) (b)

**Fig. 10** Load-slip curve of the final finite element model and pull-out test (a) steel fiber, and (b) ribbed rebar from the fiber-free cement composite and FRCC with 1% fiber

is inconsequential, resulting in brittle and sudden failure. This kind of failure is called splitting. Fig. 11 shows two different types of failures in the fiber-free cement composite specimens and the 1% FRCC.

Fig. 12 displays the von Mises stress scattering in three separate phases of fiber, rebar, and cement matrix for the FRCC specimen with 1% fiber and for a load of 32 kN. As observed, in the presence of the fibers and as a result

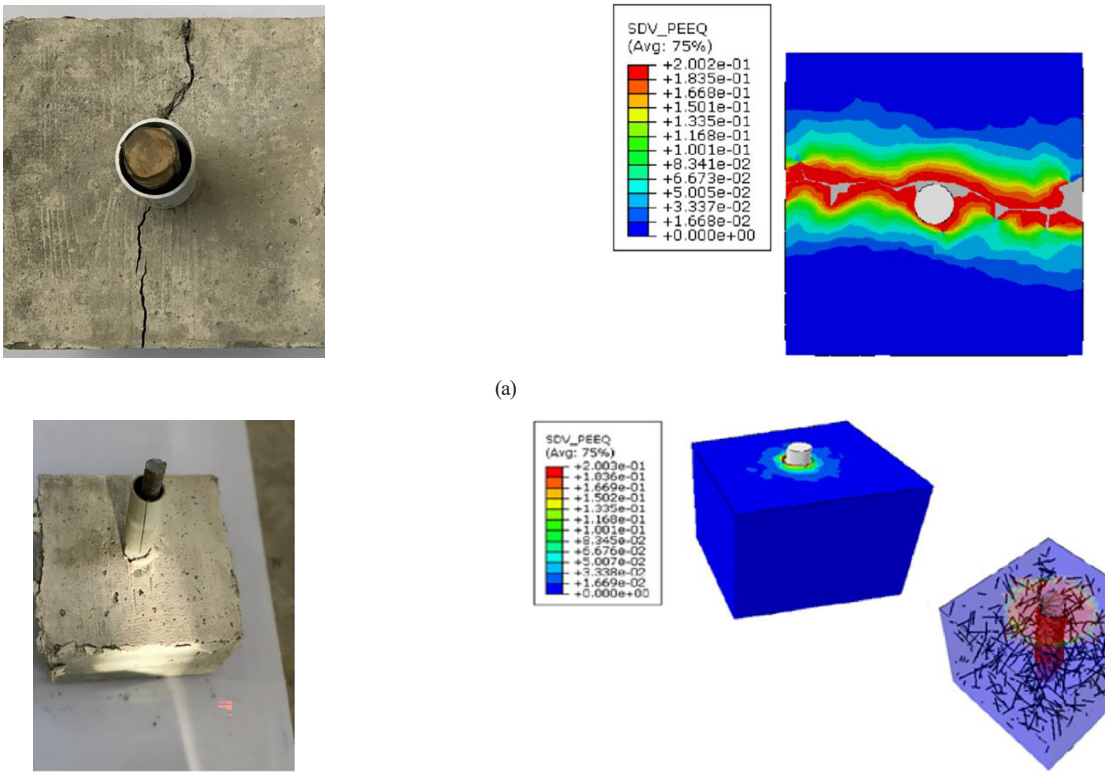


(a)

(b)

**Fig. 11** (a) Cracking path and splitting of the cement matrix for the fiber-free composite specimen (b) pull-out type failure for the FRCC specimen containing 1% fiber

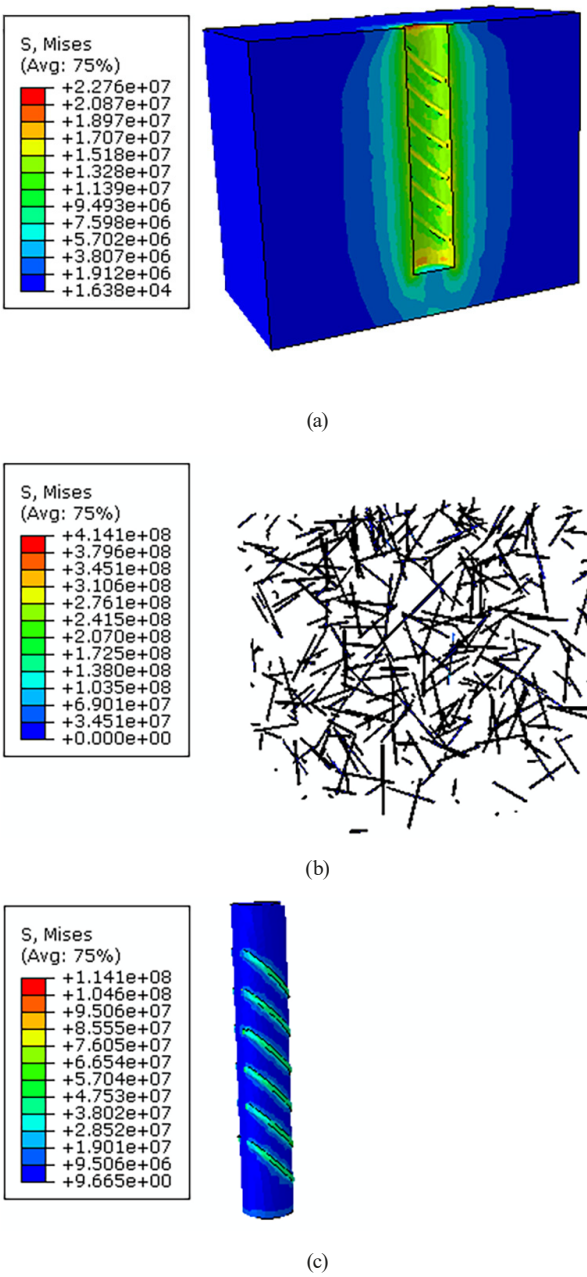


**Fig. 12** Von Mises stress distribution in three separate phases of fibers, rebar, and cement matrix for an FRCC specimen containing 1% fibers for 32 kN load: (a) steel fibers, (b) cement matrix, and (c) ribbed rebar

of bridging between the fibers and the cement matrix, the load applied to the cement matrix is distributed in the fibers. Hence, considerable stresses are generated in the fibers. As an example, in this particular case, the maximum stresses created in the three separate phases of fiber, rebar, and cement matrix are 414.1 MPa, 114.1 MPa, and 22.7 MPa, respectively. Therefore, it is seen that the fibers get a substantial portion of the transfer load to the cement matrix. Consequently, they greatly improve the mechanical properties of the cement matrix and its bond behavior with the rebar. Given the stress distribution in the ribbed rebar illustrated in Fig. 12, it can be observed that due to the greater mechanical restraint of the rebar with the cement matrix, the maximum stress created in the rebar is at the rib location. In general, the presence of fibers increases the flexibility of concrete, and by creating mechanical fasteners, they delay the growth of cracks in concrete samples containing fibers. Accordingly, the presence of fibers will improve the mechanical characteristics of concrete. In addition, the role of fibers inside the concrete is like a bridge, and by creating a bridging action, it causes the force to be transferred to its adjacent areas. This also strengthens the mechanical characteristics of concrete.

Fig. 13 shows the load-slip of the numerical model of the pull-out of the ribbed rebar and the FRCC containing 2% of fibers. It can be detected that the pull-out behavior can be separated into five major stages. At the start of loading, chemical adhesion and friction between the rebar and the composite are overcome. In the second stage, after overcoming the chemical adhesion, the rebar and the FRCC undergo relative slippery. As the loading increases, and when the load reaches the critical load $F_{cr}$ (splitting bond) of 37.7 kN, radial separation around the rebar begins. When the load reaches the ultimate bond load equal to 40 kN ($F_u$ ultimate bond), the concrete at the ribs space is completely broken, and the bond between the rebar and the concrete is lost. At this point, the bond load dramatically decreases, while the slip increases. In the fifth stage, when the slip reaches the value of $\delta_f$, the mechanical bond between the rebar and the cement matrix is completely lost, and only the surrounding friction is an influential element. Among the bond mechanisms, the mechanical bond of the ribbed rebar with the concrete is of utmost significance since it generates the highest bond tension. In this

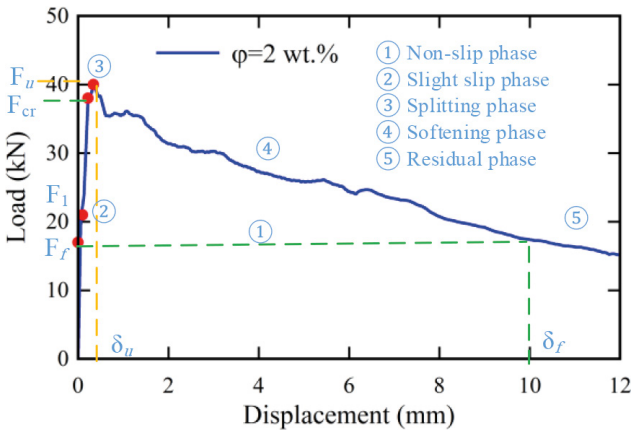


**Fig. 13** Load-slip curve of the final finite element pull-out model with 2% fiber

bond mechanism, the load transfer is performed by engaging rebar ribs and cement matrix. Consequently, compressive stress is created at the junction of rebar and concrete.

Fig. 14 shows the failure distribution and the way of pulling out the ribbed rebar from the FRCC with 2% of fibers in three zones of chemical adhesive, mechanical bond, and maximum pull-out loads. As observed, at the beginning of applying the tensile load, first all parts of the concrete involved with the rebar undergo stress, and then by overcoming the chemical and frictional adhesive loads, the failure distribution in the concrete gradually rises. As the applied load increases, the chemical adhesive loads are eliminated, and the rebar begins to separate from the concrete. In this case, the mechanical anchorage generated in the position of the rebar ribs creates local points of load transfer between the fibers and the matrix. Hence, due to the rebar higher strength, its ribs lead to the cement matrix destruction in the areas around the rebar, which is seen in Fig. 14. Examining the pull-out behavior between the ribbed rebar and the fiber-reinforced cement composite, it is observed that depending on the frictional strength of the fibers, slip takes place outwards. Thus, in this case, the failure will be of the slipping type revealed in Fig. 14. Besides chemical adhesion and frictional stability in the ribbed rebar, the mechanical bond between the matrix and ribbed section of the rebar increases the bond strength. The shear bond of the rebar with concrete is of special significance among the bond mechanisms since it generates the highest bond stress. In this bond mechanism, the load transfer is done by engaging the rib section and the cement matrix.

Fig. 15 indicates the influence of the fiber volume fraction on the load-slip curves. The results demonstrate that the fibers volume fraction significantly affects the bond behavior, and by increasing the volume fraction, the pull-out load increases. According to the results of Fig. 15 it is observed that for the fibers volume fraction equal to 0.5% and 2%, the maximum pull-out load is 31.3 kN and 40.0 kN, respectively. This indicates an increase of about 20% and 54.4% in the pull-out load compared to the fiber-free cement composite. The results indicate that with increasing the fibers volume fraction, the effect of its addition on increasing the ultimate bond load decreases. For example, by increasing the amount of fibers from 0% to 1.5%, the ultimate bond strength increases by about 40%, while by increasing the fibers from 0.5% to 2%, the ultimate bond strength increases by 25%. In the area of mechanical bonds, the fibers increase the tensile strength of the cement. Hence, utilizing fibers in this area has the greatest effect, and in the range of shear bonds, due to the reduction of the fiber and the cement matrix interface, the effect of fibers on the pull-out load can be nearly neglected. The microscopic influence of fibers in fiber-reinforced cement composite on the failure characteristics at the interface between ribbed steel rebar and the composite material is multifaceted. Firstly, the presence of

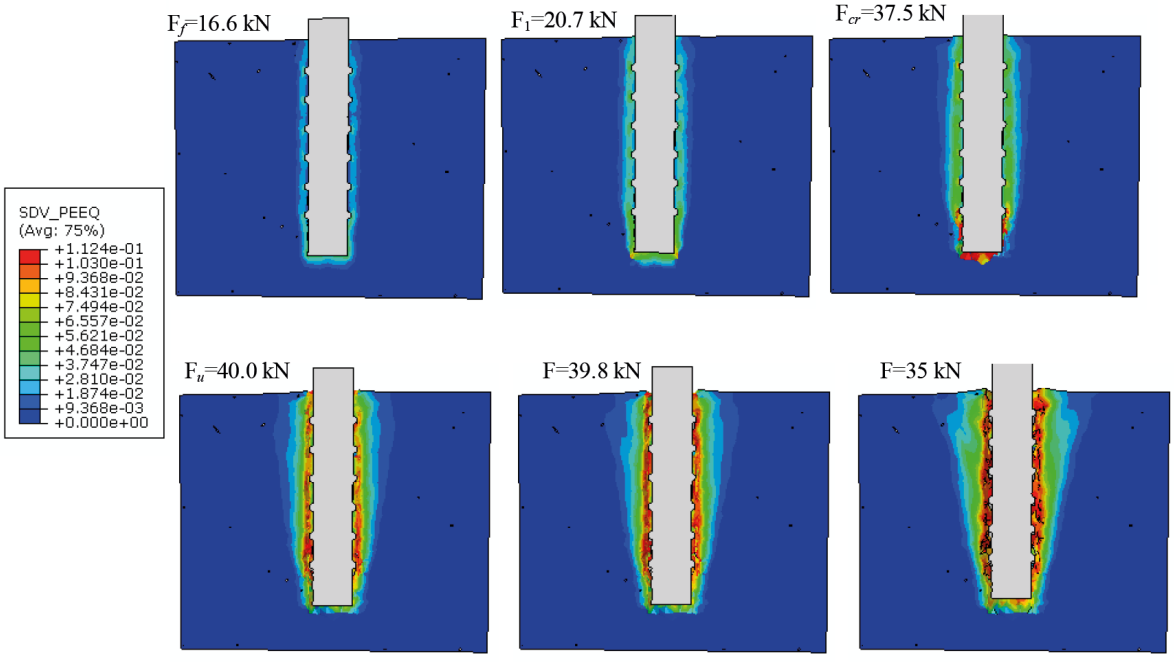


**Fig. 14** Failure distribution and the pull-out of the ribbed rebar from the FRCC with 2% of fibers at different loads

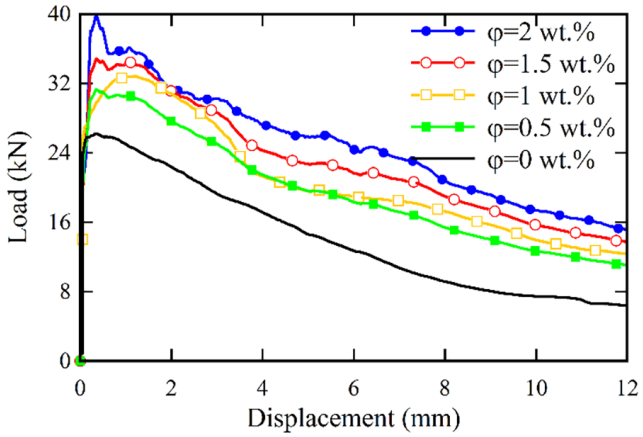


**Fig. 15** Effect of fiber content on the load-slip curve

fibers alters the stress distribution within the cementitious matrix, dispersing the applied load more evenly and reducing localized stress concentrations at the interface. This effect is particularly pronounced in areas where cracks initiate, as fibers act as bridging elements to resist crack propagation and prevent premature failure. Additionally, the fibers enhance the overall ductility of the composite, allowing for greater deformation and energy absorption before ultimate failure occurs. Moreover, the interfacial bond between the fibers and the cement matrix plays a crucial role in determining the mode of failure, with well-adhered fibers promoting cohesive failure within the composite rather than interfacial debonding. Overall, the presence of fibers in the cementitious matrix influences the failure characteristics by improving stress distribution, enhancing crack resistance, increasing ductility, and strengthening the interfacial bond, all of which contribute to a more robust and resilient interface between the rebar and the composite material.

Similar results are observed concerning the impact of rebar diameter on the bond strength based on Fig. 16. In other words, increasing the rebar diameter increases

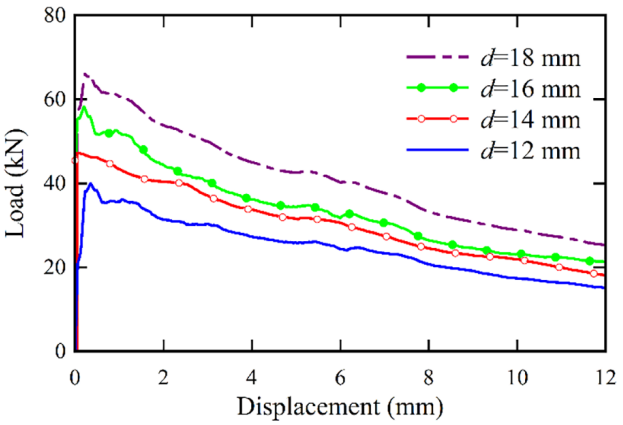


**Fig. 16** Effect of the rebar diameter on the load-slip curve

the load required to generate the bond failure. By increasing the rebar diameter, the level of bonding and mechanical engagement of the rebar and the concrete increases. Therefore, increasing the bond strength appears reasonable. For the FRCC with 2% of fibers, as the rebar diameter increases from 12 mm to 18 mm, the ultimate bond load rises from 40.0 kN to 65.8 kN, indicating an increase of approximately 65% in the pull-out load. It can be observed that when the maximum bond stress is attained, the load-bearing mechanism is lost, and the residual connection strength depends mainly on the frictional strength. Besides, according to Fig. 17, it is observed that with the increase of the fibers volume fraction used in the concrete, the maximum stress generated in the rebar increases, and the maximum stress emerges around the rebar ribs.

The pull-out load according to the slenderness ratio of steel microfibers is shown in Fig. 18 for the sample containing 1 wt.% steel fibers for the investigation of the influence of the slenderness ratio. According to Fig. 18, as the slenderness ratio increases from 10 to 47, the pull-out force increases from 32.7 kN to 34.6 kN. The pull-out force diminishes to 30.5 kN with an increase in slenderness ratio beyond this range. Because slenderness increases with fiber length, for larger values of slenderness coefficients the probability of accumulation of steel fibers increases, leading to the development of cracks in these areas. The results indicate that, in optimal conditions, steel fibers have a slenderness coefficient of 47, which causes the pull-out force to reach its maximum. Changes in the volume fraction of fibers in fiber-reinforced cement composite profoundly impact pull-out properties through various intrinsic mechanisms. Firstly, an increased fiber volume fraction enhances bonding by providing more opportunities for fibers to come into contact with the rebar surface, thereby enhancing mechanical interlocking and frictional resistance. Secondly, higher fiber volume fractions contribute to crack bridging within the cementitious matrix, forming a denser network of reinforcement that can distribute stress and prevent crack propagation. Additionally, the increased ductility associated with higher fiber volume fractions allows for better crack deflection and energy dissipation, reducing localized stress concentrations around the rebar interface and mitigating premature failure. Moreover, the quality and strength of the interfacial bond between fibers and the matrix are influenced by the fiber volume fraction, with proper dispersion and orientation leading to improved load transfer and enhanced pull-out properties overall. These intrinsic mechanisms

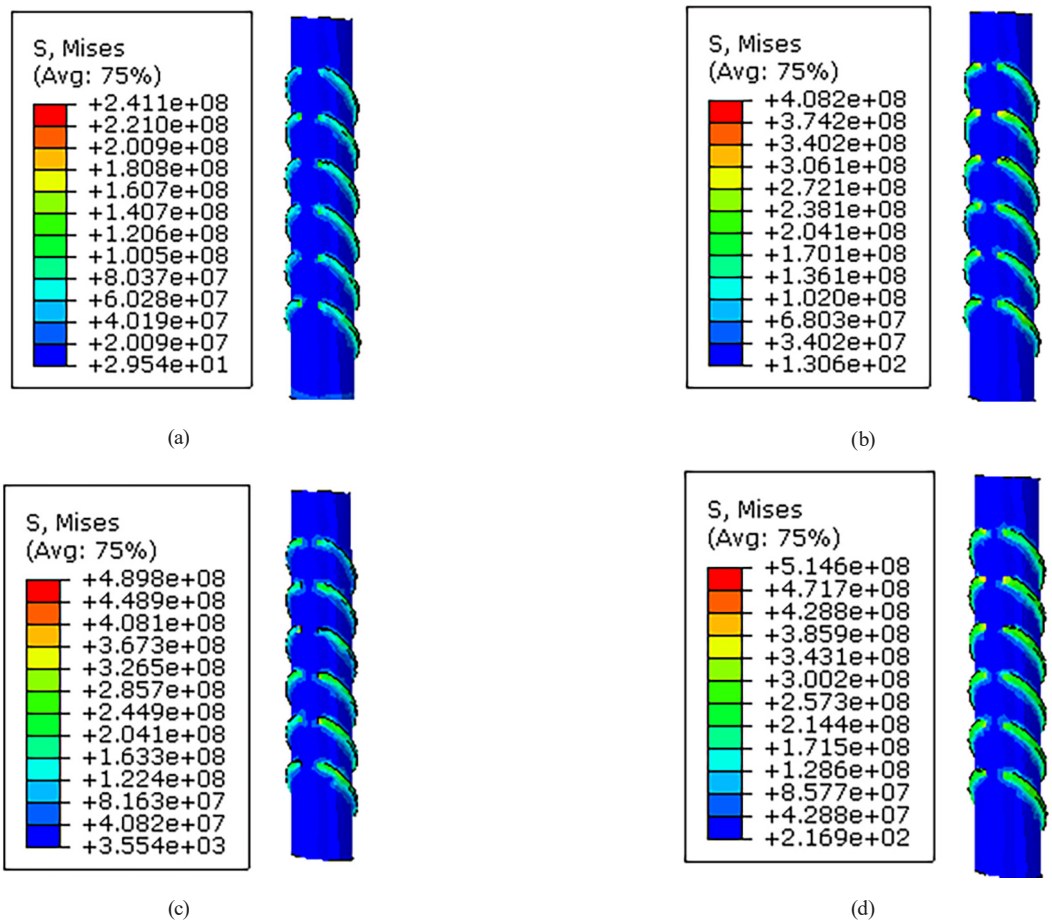


**Fig. 17** Stress distribution in the rebar located in the FRCC containing: (a) 0% fibers, (b) 1% fibers, (c) 1.5% fibers and (d) 2% fibers

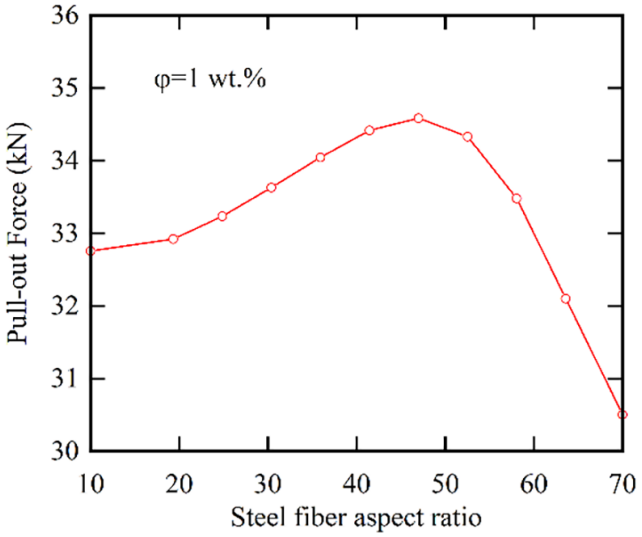


**Fig. 18** Pull-out force in terms of slenderness ratio for the sample containing 1 wt.% steel fibers

highlight the complex interplay between fiber characteristics, matrix properties, and interface behavior, all of which significantly affect the pull-out performance of the composite material.

To precisely examine the influence of parameters on the bond characteristics, Table 4 shows the effect of the rebar diameter and the fibers volume fraction on the pull-out response, containing pull-out load, slip related to maximum load, pull-out energy, effective pull-out stress, and pull-out work in each model. The outcomes reveal that the pull-out load and the total pull-out work (area under the load-slip curve) increase with increasing the fibers diameter and volume fraction. Moreover, it is detected that for the rebar with a diameter of 18 mm, accumulative the fiber content from 0 to 2%, the pull-out load and work increase by 55% and 72%, respectively. Furthermore, it is observed that the bond strength decreases with increasing the rebar diameter. Bond strength is determined as the ratio of the pull-out load to the area of the buried surface of the rebar ($\sigma = P/A$), where $P$ is the pull-out load and $A$ is the buried surface area of the rebar. Nonetheless, the opposite is true for the volume fraction of the fibers, and as the fibers volume fraction increases, the bond stress also increases. Thus, it can be decided that the utilization of steel fibers substantially increases the pull-out between the rebar and the concrete.

**Table 4** Influence of the rebar diameter and fiber content on pull-out load, critical separation, pull-out energy, and average bond strength

| Fiber content (%) | Bar diameter, (mm) | Pull-out load (kN) | Critical separation (mm) | Pull-out work (MPa·mm) | Effective bond strength (MPa) |
|---|---|---|---|---|---|
| 0 | | 26.1 | 0.211 | 170 | 230.89 |
| 0.5 | | 31.2 | 0.336 | 238 | 276.01 |
| 1 | 12 | 33.1 | 0.945 | 259 | 292.82 |
| 1.5 | | 36.8 | 0.389 | 276 | 325.55 |
| 2 | | 40.0 | 0.301 | 314 | 353.86 |
| 0 | | 29.5 | 0.131 | 208 | 191.73 |
| 0.5 | | 33.7 | 0.243 | 265 | 219.03 |
| 1 | 14 | 38.9 | 0.431 | 287 | 252.83 |
| 1.5 | | 41.4 | 0.163 | 341 | 269.08 |
| 2 | | 47.8 | 0.039 | 376 | 310.67 |
| 0 | | 36.8 | 0.235 | 247 | 183.12 |
| 0.5 | | 41.7 | 0.341 | 334 | 207.50 |
| 1 | 16 | 45.0 | 0.531 | 385 | 223.93 |
| 1.5 | | 52.7 | 0.321 | 416 | 262.24 |
| 2 | | 58.3 | 0.181 | 425 | 290.11 |
| 0 | | 42.6 | 0.240 | 287 | 167.49 |
| 0.5 | | 58.9 | 0.308 | 358 | 231.58 |
| 1 | 18 | 61.5 | 0.435 | 398 | 241.80 |
| 1.5 | | 62.3 | 0.284 | 457 | 244.95 |
| 2 | | 66.4 | 0.243 | 495 | 261.07 |

## 5 Conclusions

This study investigated the pull-out behavior between the ribbed rebar and the FRCC using the meso-scale finite element method. The interaction among the fibers, the rebar, and the cement matrix is simulated by using the ITZ model. Its parameters have been acquired utilizing the inverse numerical method and the results of the experimental rebar pull-out test. After validating the results of the finite element models with the experimental test results, the effect of the fibers diameter and volume fraction on the bond response between the ribbed rebar and the FRCC was investigated. The results show that better bond strength is obtained by increasing the fibers volume fraction. Besides, the maximum pull-out load increases as the rebar diameter and the fibers volume fraction increase. This is due to the mechanical mechanisms created by the interaction of the fibers and the cement matrix, as well as the increase in mechanical stress due to the load component perpendicular to the fibers length and the presence of the rebar ribs. The results of the present study reveal that the proposed finite element method can predict the pull-out behavior of rebar from FRCC precisely.

## Acknowledgment

We acknowledge Semnan Branch, Islamic Azad University for financial support.

## Author contributions

AM provided the basic idea and revised the paper. RA performed the literature search, analyzed the data, and drafted the paper. AB contributed to the further literature search and revising. All the authors read and approved the manuscript.

## Authors' information

Reza Akbarifar is a Ph.D. candidate in Structural Engineering, Civil Engineering Department, Semnan Branch, Islamic Azad University, Semnan, Iran. His research interests include the bond behavior of fiber-reinforced concrete and ECC.

Alireza Mortezaei is a Professor, Seismic Geotechnical and High-Performance Concrete Research Centre, Civil Engineering Department, Semnan Branch, Islamic Azad University, Semnan, Iran. His research interests lie in the Structural Dynamics and Nonlinear Behavior of FRC, FRCC, and RC Structures under the Near-Fault Ground Motions, rehabilitation of buildings, and seismic design of RC structures.

Ali Babaei is an Assistant Professor, at the Department of Civil Engineering, Semnan University, Semnan, Iran. His research interests include the design of reinforced concrete structures.

## Competing interests

The authors declare that they have no conflict of interest.

## References

[1] Izadpanah, S., Shooshpasha, I., Hajiannia, A. "The impact of zeolite on mineralogy changes and compressive strength development of cement-treated sand mixtures through microstructure analysis", Scientia Iranica, 28(3), pp. 1182–1194, 2021. https://doi.org/10.24200/sci.2020.55431.4218

[2] Khosravi, S., Goudarzi, M. A. "Seismic risk assessment of on-ground concrete cylindrical water tanks", Innovative Infrastructure Solutions, 8(1), 68, 2023. https://doi.org/10.1007/s41062-022-01002-8

[3] Masaeli, H., S. Khosravi, and H. Choobkar, "Effects of superplasticizer and antifreeze additives on strength and permeability properties of pervious concrete based on experiments", Journal of Experimental Research in Civil Engineering, 4(7), pp. 49–60, 2018.

[4] Esmaeili, J., Andalibi, K., Gencel, O. "Mechanical characteristics of experimental multi-scale steel fiber reinforced polymer concrete and optimization by Taguchi methods", Construction and Building Materials, 313, 125500, 2021.
https://doi.org/10.1016/j.conbuildmat.2021.125500

[5] Gencel, O., Kazmi, S. M. S., Munir, M. J., Kaplan, G., Bayraktar, O. Y., Yarar, D. O., Karimipour, A., Ahmad, M. R. "Influence of bottom ash and polypropylene fibers on the physico-mechanical, durability and thermal performance of foam concrete: An experimental investigation", Construction and Building Materials, 306, 124887, 2021.
https://doi.org/10.1016/j.conbuildmat.2021.124887

[6] Gencel, O., Brostow, W., Datashvili, T., Thedford, M. "Workability and mechanical performance of steel fiber-reinforced self-compacting concrete with fly ash", Composite Interfaces, 18(2), pp. 169–184, 2011.
https://doi.org/10.1163/092764411X567567

[7] Xie, C., Cao, M., Khan, M., Yin, H., Guan, J. "Review on different testing methods and factors affecting fracture properties of fiber reinforced cementitious composites", Construction and Building Materials, 273, 121766, 2021.
https://doi.org/10.1016/j.conbuildmat.2020.121766

[8] Hajforoush, M., Kheyroddin, A., Rezaifar, O., Kioumarsi, M. "The effects of uniform magnetic field on the mechanical and microstructural properties of concrete incorporating steel fibers", Scientia Iranica, 28(5), pp. 2557–2567, 2021.
https://doi.org/10.24200/sci.2021.56888.4963

[9] Esmaeili, J., Aghdam, O. R., Andalibi, K., Kasaei, J., Gencel, O. "Experimental and numerical investigations on a novel plate anchorage system to solve FRP debonding problem in the strengthened RC beams", Journal of Building Engineering, 45, 103413, 2022.
https://doi.org/10.1016/j.jobe.2021.103413

[10] Esmaeili, J., Khoshkanabi, S. P., Andalibi, K., Kasaei, J. "An innovative method for improving the cyclic performance of concrete beams retrofitted with prefabricated basalt-textile-reinforced ultra-high performance concrete", Structures, 52, pp. 813–823, 2023.
https://doi.org/10.1016/j.istruc.2023.04.004

[11] Esmaeili, J., Romouzi, V., Kasaei, J., Andalibi, K. "An investigation of durability and the mechanical properties of ultra-high performance concrete (UHPC) modified with economical graphene oxide nano-sheets", Journal of Building Engineering, 80, 107908, 2023.
https://doi.org/10.1016/j.jobe.2023.107908

[12] Esmaeili, J., Sharifi, I., Andalibi, K., Kasaei, J. "Effect of different matrix compositions and micro steel fibers on tensile behavior of textile reinforced concrete", IOP Conference Series: Materials Science and Engineering, 246, 012031, 2017.
https://doi.org/10.1088/1757-899X/246/1/012031

[13] Emami, F., Kabir, M. Z. "Performance of composite metal deck slabs under impact loading", Structures, 19, pp. 476–489, 2019.
https://doi.org/10.1016/j.istruc.2019.02.015

[14] Garcia-Taengua, E., Martí-Vargas, J. R., Serna, P. "Bond of reinforcing bars to steel fiber reinforced concrete", Construction and Building Materials, 105, pp. 275–284, 2016.
https://doi.org/10.1016/j.conbuildmat.2015.12.044

[15] Pi, Z., H. Xiao, R. Liu, M. Liu, and H. Li, "Effects of brass coating and nano-$SiO_2$ coating on steel fiber–matrix interfacial properties of cement-based composite, Composites Part B: Engineering, 189, 107904, 2020.
https://doi.org/10.1016/j.compositesb.2020.107904

[16] Lin, A., Ostertag, C. P. "Interaction between high performance fiber reinforced cement-based composites and steel reinforcement", Engineering Structures, 247, 113173, 2021.
https://doi.org/10.1016/j.engstruct.2021.113173

[17] Zhou, Z., Qiao, P. "Bond behavior of epoxy-coated rebar in ultra-high performance concrete", Construction and Building Materials, 182, pp. 406–417, 2018.
https://doi.org/10.1016/j.conbuildmat.2018.06.113

[18] Kamani, R., Kamali Dolatabadi, M., Asghharian Jeddi, A. A., Nasrollahzadeh, K. "Increasing the efficiency of carbon fiber bundles in reinforcing fine grained concrete: an experimental study of flexural bearing capacity", Journal of Science and Technology of Composites, 6(2), pp. 310–318, 2019.
https://doi.org/10.22068/jstc.2018.85673.1441

[19] Wang, Y., Li, Z., Zhang, C., Wang, X., Li, J., Liang, Y., Chu, S. "Bond behavior of BFRP bars with basalt-fiber reinforced cement-based composite materials", Structural Concrete, 22(1), pp. 154–167, 2021.
https://doi.org/10.1002/suco.201900548

[20] Khosravi Maleki, F., Nasution, M. K. M., Gok, M. S., Arab Maleki, V. "An experimental investigation on mechanical properties of $Fe_2O_3$ microparticles reinforced polypropylene", Journal of Materials Research and Technology, 16, pp. 229–237, 2022.
https://doi.org/10.1016/j.jmrt.2021.11.104

[21] Vahidi Pashaki, P., Pouya, M., Maleki, V. A. "High-speed cryogenic machining of the carbon nanotube reinforced nanocomposites: Finite element analysis and simulation", Proceedings of the Institution of Mechanical Engineers, Part C: Journal of Mechanical Engineering Science, 232(11), pp. 1927–1936, 2018.
https://doi.org/10.1177/0954406217714012

[22] Khosravi, S., Yousefi, M. M., Goudarzi, M. "Development of seismic fragility curves of cylindrical concrete tanks using nonlinear analysis", Amirkabir Journal of Civil Engineering, 53(1), pp. 71–88, 2021.
https://doi.org/10.22060/ceej.2021.19121.7079

[23] Altas, E., F. Khosravi, H. Gokkaya, V.A. Maleki, Y. Akınay, O. Ozdemir, O. Bayraktar, and H. Kandas, "Finite element simulation and experimental investigation on the effect of temperature on pseudoelastic behavior of perforated Ni–Ti shape memory alloy strips", Smart Materials and Structures, 31(2), 025031, 2022.
https://doi.org/10.1088/1361-665X/ac4691

[24] Jamali, S., Zare, Y., Rhee, K. Y. "Modeling of mechanical behaviors and interphase properties of polymer/nanodiamond composites for biomedical products", Journal of Materials Research and Technology, 19, pp. 2750–2758, 2022.
https://doi.org/10.1016/j.jmrt.2022.06.007

[25] Razi, S., Wang, X., Mehreganian, N., Tootkaboni, M., Louhghalam, A. "Application of mean-force potential lattice element method to modeling complex structures", International Journal of Mechanical Sciences, 260, 108653, 2023.
https://doi.org/10.1016/j.ijmecsci.2023.108653

[26] Naderi, S., Zhang, M. "3D meso-scale modelling of tensile and compressive fracture behaviour of steel fibre reinforced concrete", Composite Structures, 291, 115690, 2022.
https://doi.org/10.1016/j.compstruct.2022.115690

[27] Eslami, E., Zhou, L., Yun, H.-B. "Noncontact Absolute Stress Measurement for UHPC Using Raman Piezospectroscopy", In: Transportation Research Board 98th Annual Meeting, Washington, DC, USA, 2019, 19-00976.

[28] Yun, H.-B., Eslami, E., Zhou, L. "Noncontact stress measurement from bare UHPC surface using Raman piezospectroscopy", Journal of Raman Spectroscopy, 49(9), pp. 1540–1551, 2018.
https://doi.org/10.1002/jrs.5401

[29] Ghaderi, M., Maleki, V. A., Andalibi, K. "Retrofitting of unreinforced masonry walls under blast loading by FRP and spray on polyurea", Cumhuriyet University Faculty of Science, 36(4), pp. 462–477, 2015.

[30] Esmaeili, J., Andalibi, K., Gencel, O., Maleki, F. K., Maleki, V. A. "Pull-out and bond-slip performance of steel fibers with various ends shapes embedded in polymer-modified concrete", Construction and Building Materials, 271, 121531, 2021.
https://doi.org/10.1016/j.conbuildmat.2020.121531

[31] Komasi, M., Khosravi, S., Chobkar, H. "Laboratory study for optimal mixing scheme of pervious concrete containing additive of microsilica fume based on maximum compressive strength and permeability", Journal of Structural and Construction Engineering, 7(4), pp. 42–61, 2020.
https://doi.org/10.22065/jsce.2018.135444.1586

[32] Khani, N., Yildiz, M., Koc, B. "Elastic properties of coiled carbon nanotube reinforced nanocomposite: A finite element study", Materials & Design, 109, pp. 123–132, 2016.
https://doi.org/10.1016/j.matdes.2016.06.126

[33] Esmaeili, J., Andalibia, K. "Development of 3D Meso-Scale finite element model to study the mechanical behavior of steel microfiber-reinforced polymer concrete", Computers and Concrete, 24(5), pp. 413–422, 2019.
https://doi.org/10.12989/cac.2019.24.5.413

[34] Ayatollahi, M. R., Shadlou, S., Shokrieh, M. M. "Multiscale modeling for mechanical properties of carbon nanotube reinforced nanocomposites subjected to different types of loading", Composite Structures, 93(9), pp. 2250–2259, 2011.
https://doi.org/10.1016/j.compstruct.2011.03.013

[35] Yao, Y., Zhang, H., Zhang, X., Ren, F., Li, Y., Yang, Z. "Experimental, Analytical and Numerical Studies of Interfacial Bonding Properties between Silane-Coated Steel Fibres and Mortar", Buildings, 11(9), 398, 2021.
https://doi.org/10.3390/buildings11090398

[36] Alizadeh, M. H., Ajri, M., Maleki, V. A. "Mechanical properties prediction of ductile iron with spherical graphite using multi-scale finite element model", Physica Scripta, 98(12), 125270, 2023.
https://doi.org/10.1088/1402-4896/ad0d97

[37] Bouhala, L., Makradi, A., Belouettar, S., Younes, A., Natarajan, S. "An XFEM/CZM based inverse method for identification of composite failure parameters", Computers & Structures, 153, pp. 91–97, 2015.
https://doi.org/10.1016/j.compstruc.2015.02.035

[38] Chao, S.-H., Naaman, A. E., Parra-Montesinos, G. J. "Bond behavior of strand embedded in fiber reinforced cementitious composites", PCI Journal, 51(6), pp. 56–71, 2006.
https://doi.org/10.15554/pcij.11012006.56.71

[39] ASTM "ASTM C496/C496M-17 Standard Test Method for Splitting Tensile Strength of Cylindrical Concrete Specimens", ASTM International, West Conshohocken, PA, USA, 2017.
https://doi.org/10.1520/C0496_C0496M-17

[40] INSO "ISIRI 3132 Hot rolled steel bars for concrete reinforcement - Specification and test methods", Iran National Standards Organization, Karaj, Alborz, Iran, 2013.

[41] ASTM "ASTM A615/A615M-24 Standard Specification for Deformed and Plain Carbon-Steel Bars for Concrete Reinforcement", ASTM International, West Conshohocken, PA, USA, 2024.
https://doi.org/10.1520/A0615_A0615M-24

[42] ASTM "ASTM E8/E8M-24 Standard Test Methods for Tension Testing of Metallic Materials", ASTM International, West Conshohocken, PA, USA, 2024.
https://doi.org/10.1520/E0008_E0008M-24

[43] RILEM TC "RC6 Bond test reinforcement steel. 2. Pull-out Test, 1983", In: RILEM Recommendations for the Testing and Use of Constructions Materials, E & FN Spon, 1994, pp. 218–220. ISBN 2351580117
https://doi.org/10.1617/2351580117.081

[44] Du, C., Sun, Y., Chen, J., Gong, H., Wei, X., Zhang, Z. "Analysis of cohesive and adhesive damage initiations of asphalt pavement using a microstructure-based finite element model", Construction and Building Materials, 261, 119973, 2020.
https://doi.org/10.1016/j.conbuildmat.2020.119973

[45] Naderi, S., Tu, W., Zhang, M. "Meso-scale modelling of compressive fracture in concrete with irregularly shaped aggregates", Cement and Concrete Research, 140, 106317, 2021.
https://doi.org/10.1016/j.cemconres.2020.106317